

DesignCon 2011

Inter-Dependence of Dielectric and Conductive Losses in Interconnects

Gustavo Blando, Oracle Corporation

Tel: (781) 442 2779, e-mail: gustavo.blando@oracle.com

Leandro Cagliero, Famaf-Conicet, Univ Nac Cordoba, Argentina

Jason R. Miller, Oracle Corporation Inc

Roger Dame, Oracle Corporation Inc

Kevin Hinckley, Oracle Corporation Inc

Douglas Winterberg, Oracle Corporation, Inc

Joe Beers, Gold Circuit Electronics

Istvan Novak, Oracle Corporation, Inc

Abstract

With the recent advances of multi-gigabit signaling schemes, the proper modeling of lossy and dispersive interconnects is becoming more and more important. For system design and laminate-procurement reasons it is desirable to have separate specifications and modeling parameters for the dielectric laminate and copper. Unfortunately the different standard test methodologies very often yield different results for the same materials. This becomes particularly obvious when dielectric losses are compared from bare dielectrics and finished printed circuit boards. The difference is often attributed to surface roughness. Beyond empirical data, however, no physical explanation and modeling has been published to explain this difference.

This paper will show a methodology to measure and post process S-parameters in order to directly obtain the underlying RLGC parameters. This way, applying no, or minimum fitting, we'll have a notion and understanding of where the losses are coming from

Author(s) Biography

Gustavo Blando is a Principle Engineer, with over 15 years of experience in the industry. Currently at Oracle Corporation he is responsible for the development of new processes and methodologies in the areas of broadband measurement, high speed modeling and system simulations. He received his M.S. from Northeastern University.

Leandro Cagliero is a faculty member at Famaf-Conicet, (Universidad Nacional de Cordoba, Argentina) with over 15 years of teaching experience in the fields of representation theory with Lie groups. He's an active research member of CONICET with multiple scientific publications in different areas of pure mathematics. He's currently visiting lecturer and research scholar at the MIT math department. He's received his PhD in mathematics from FAMAF and Post-doc at MIT.

Jason R. Miller is a Principle Hardware Engineer at Oracle Corporation where he works on ASIC development, ASIC packaging, interconnect modeling and characterization, and system simulation. He has published over 40 technical articles on the topics such as high-speed modeling and simulation and co-authored the book "Frequency-Domain Characterization of Power Distribution Networks" published by Artech House. He received his Ph.D. in electrical engineering from Columbia University.

Roger Dame is a Principle Hardware Engineer at Oracle Corporation where he works on mid-ranged servers, SI work in general, simulation, and lab work. He has 34 years of experience on analog, digital design and signal integrity work with DEC, Compaq, and HP. He received his B.S. in electrical engineering from CNEC.

Kevin Hinckley is a Signal Integrity Engineer at Oracle Corporation with more than 15 years in the industry. Current responsibilities include all aspects of signal integrity modeling, analysis and validation within Sun's x64 server division. Prior to his time at Sun, Kevin worked in the Defense Industry with a focus on semiconductor device modeling, simulation and measurement. He received a BSEE from Rensselaer Polytechnic Institute.

Douglas Winterberg is a Signal Integrity Engineer at Oracle Corporation with over 10 years experience in systems and interconnect design. Currently he works on system modeling, simulations and validation of high speed interconnects on Sun's time to market server platforms. He received his BS from the Rochester Institute of Technology.

Joe Beers is VP of Sales at Gold Circuit Electronics with 27 years experience in the manufacture of printed circuit boards and varied experiences as a laboratory chemist, process and product engineer, quality director and manufacturing leader. In his current position with Gold Circuit Electronics for the last 10 years, he has held a variety of positions namely in the area of engineering and quality support and strong cooperation technically with OEM customers, including capability assessment and material testing, specific focus on materials and processes, coupled with quality management and field experience. Joe graduated with a chemistry degree from Adelphi University in New York. Thermal analysis, DOE and statistical analysis training ensued professionally.

Istvan Novak is a Senior Principle Engineer at Oracle. Besides signal integrity design of high-speed serial and parallel buses, he is engaged in the design and characterization of power-distribution networks and packages for mid-range servers. He creates simulation models, and develops measurement techniques for power distribution. Istvan has twenty plus years of experience with high-speed digital, RF, and analog circuit and system design. He is a Fellow of IEEE for his contributions to signal-integrity and RF measurement and simulation methodologies.

1.0 Introduction

With the recent advances of multi-gigabit signaling schemes, the proper modeling of lossy and dispersive interconnects is becoming more and more important. The simplest model of an electrically long transmission line is the T-line model, which assumes no losses and captures the frequency independent characteristic impedance and propagation delay. Adding either conductive or dielectric losses, the transmission behavior of the interconnect will become dispersive. The popular W-line model, introduced in the mid 90s, capture an almost-causal set of conductive losses and a non-causal dielectric loss. With the generic RLGC ladder equivalent circuit one can make causal models by modeling each of the R, L, G and C per-unit-length parameters as an appropriate function of frequency. Conductive losses also have to capture the surface roughness of the conductors, which traditionally were modeled with the Hammerstad model.

For system design and laminate-procurement reasons it is desirable to have separate specifications and modeling parameters for the dielectric laminate and copper. There are a multitude of IPC standards to measure the electrical properties of printed circuit board dielectric and conductive materials. Unfortunately the different methodologies often yield different results for the very same materials. This becomes particularly obvious when dielectric losses are compared from bare dielectrics and finished printed circuit boards [1]. For several high-speed laminates the bare dielectric loss measured by microwave cavities shows a relatively slow rise or fall of dielectric loss as a function of frequency. In contrast, the same material measured with the Short Pulse Propagation method will show a much steeper rise of dielectric loss with frequency. The difference is often attributed to surface roughness or to the interface layer between the copper and dielectric. Beyond empirical data, however, no physical explanation and modeling has been published to explain this difference.

This paper will show a methodology to measure and correct S-parameters in order to directly obtain the underlying RLGC parameters. This way, by applying no, or minimum fitting, we'll improve our understanding of "where" the losses are coming from

2.0 Current Methods Used to Derive Dielectric and Conductive Losses

Several methods have been proposed over the years to measure/derive dielectric losses. The majority of these procedures, measure only the dielectric alone, and then, the conductive losses are computed with the help of simulation models. Later proposed methods are based on complete pressed stack measurement including both dielectric and conductive losses; the challenge on these method lies in separating conductive from dielectric losses in the post-processing steps.

One way or the other, in order to obtain a complete picture of a transmission line with both conductive and dielectric losses, all these methods rely on simulation models, either to obtain or to separate its elements, none of them can directly measure/derive RLGC.

For dielectric measurements, fabricators have been using for instance the Parallel Plate (PP) or stripline methods. The PP method uses the bare dielectric between test electrodes and the setup measures the plate capacitor formed by this structure [1]. The stripline method creates a transmission line formed by metal strips and planes and the dielectric slabs to be measured [2].

In recent years methods based on finished printed circuit board traces have become popular. The Short Pulse Propagation method (Section 1.3 of [3]), the Root Impulse Energy (Section 1.2 of [3]), Equivalent Bandwidth method (Section 1.1 of [3]) and the SET2DIL [4] method are the most common.

SPP works on the complete pressed stack. The idea is to measure two different lengths of the nominally same transmission line in the time domain, then after a few waveform manipulations, convert them to the frequency

domain and compute the attenuation. As a post-processing step after a cross-section is performed, the trace has to be modeled in a 2D field solver to compute the simulated attenuation. Different loss tangent values are used as inputs to the field solver until the simulated results matches the measured attenuation. The lost tangent is found when a good match is achieved between the measured and the simulated attenuation output. It's implied that if the 2-D cross-section structure model does not include any surface imperfection, the resulting loss tangent will include the effect of surface roughness. Additionally since loss tangent is an input to the solver, many different loss-tangent shapes can be derived that will produce a good attenuation match [5].

Figure 1 shows dielectric loss results obtained with three different measurement techniques superimposed in the same plot. SPP shows a steep slope. The PP method shows a slightly negative slope that goes from 1MHz to 1GHz. Finally, there is a single point at 10GHz taken from the cavity method. A detailed explanation of the measurement method and results for this figure can be found in [6]

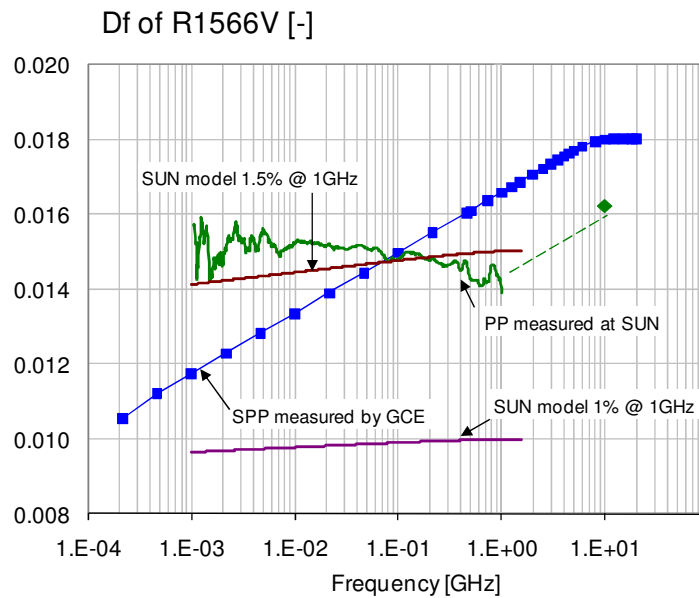


Figure 1: Dielectric Loss obtained by different measurement and simulation techniques (from [6])

Additionally on the same figure the widely accepted and used wide-band multi pole Debye model [7] (called Sarkar model on the coming figures) have been superimposed assuming a loss tangent of 1.5% and 1% at 1GHz.

By reflecting on the previous figure we are left wondering what is then, the real loss tangent of this material? Clearly the various curves are different enough that we can't identify a trend, furthermore surface roughness is not included explicitly, even though we think it is possible it's already included (together with loss tangent) on the SPP data.

SPP is based on matching measurement to simulations, so if the final matching is good we can conclude that the results are correct. There are two points to consider about this argument:

- What is the meaning of "good" match? Often times this is done just by observation of overlaid traces on a plot. Other methods can be used, for example minimum least square, to come up with a metric. But ultimately the goodness or badness of the match will be subjected to the interpretation and experience of the user taking or analyzing the measurement data
- How many solutions create a "good" match? This is an important point, since in most of these simulations/problems we have at least two and sometimes more variables to tune. Specifically in our case we could tune dielectric losses and/or surface roughness. For these cases it's easy to show that there are many solutions (in theory infinite) that would result in a "good match"

To see this more clearly, two transmission line models were created. One, using the loss-tangent curve obtained from SPP, and the other using the wide-band Debye [2] loss tangent extrapolation model. The SPP transmission line model was kept the same, while the wide-band Debye (Sarkar) model was swept changing both loss-tangent and surface roughness (In this example a Hammerstad [8] surface roughness model was used).

For this experiment we define the concept of a "match" as the difference in area over the frequency range between insertion losses of the different cases. This metric gives a single number, the smaller the number the better the matching over the frequency range [0-20GHz]. In *Figure 2* (Top-left) an example of insertion loss curve for both models can be seen. With the above definition, the difference between the insertion loss curves is the integral of the area in the top right plot.

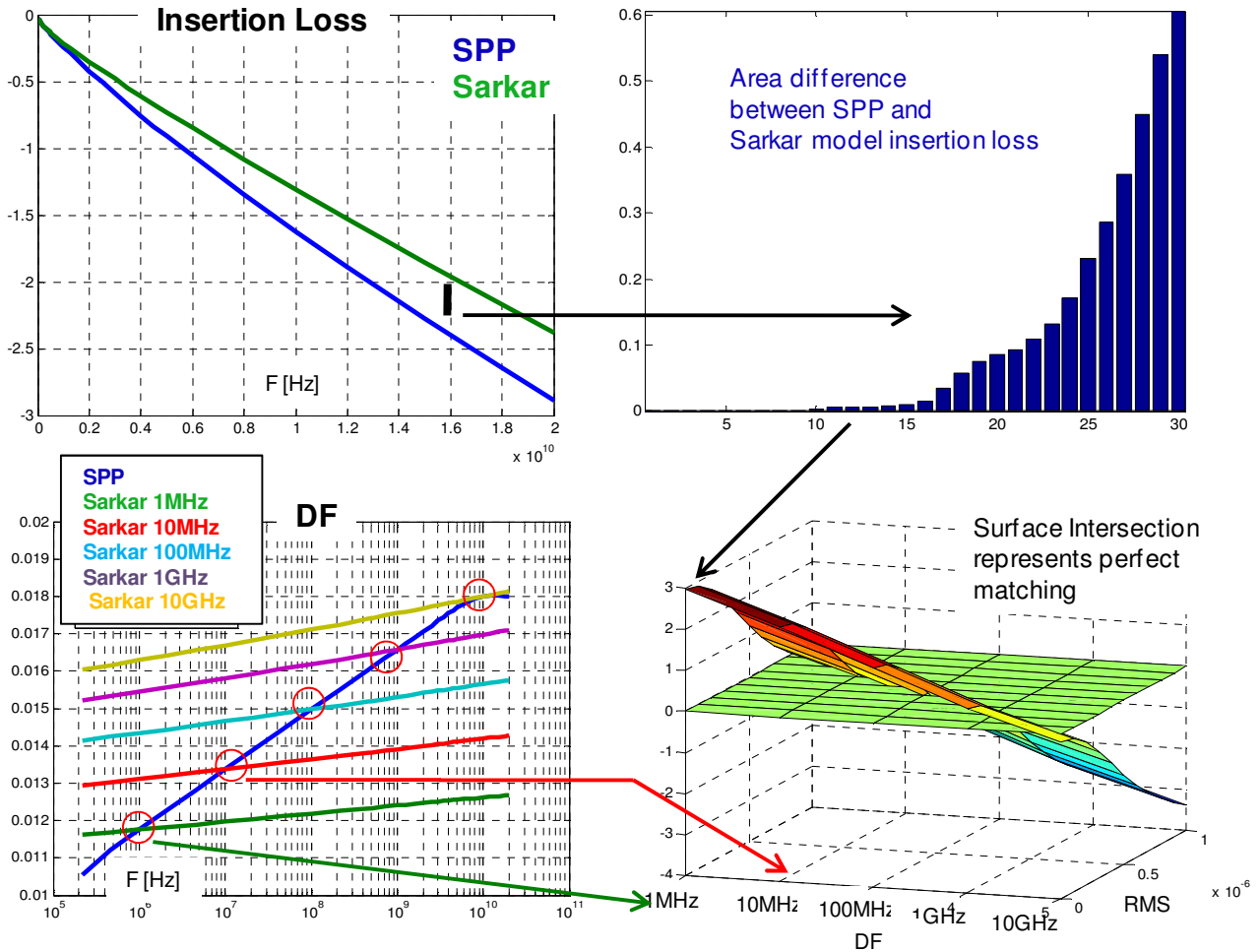


Figure 2:(Top-left) Insertion loss for SPP and Sarkar-model, (Top-right) area difference over frequency between SPP and Sarkar-model, (Bottom-left) Df model for SPP vs. different variants of Sarkar, (Bottom-right), surface sensitivity while sweeping the different Sarkar models vs RMS surface roughness as compared to the SPP result

Many models were created with different surface roughness and loss tangent values. *Figure 2* (Bottom-left) shows the discrete loss-tangent values used to generate the models on the sweep. Surface roughness was swept between 0 and 1um RMS. *Figure 2* (Bottom-Right) shows the surface with parameter sensitivity against a "good match" as defined above. The intersection of this surface with the zero plane, represents perfect matching. The surface looks almost 45 degree. This means the sensitivity of surface roughness is very similar to that of the loss tangent. In other words, this is telling us that there are many (infinite) solution to this problem as shown by the intersection of these two curves, and also it's telling us that the sensitivity of these two parameters (loss tangent and surface roughness) are approximately the same.

We go back then to the same fundamental question: What is then the real value of loss tangent and surface roughness for this sample? Simply put, we don't know!!!!

With this in mind, we attempted to obtain RLGC parameters directly from measurements, with minimum or no fitting. RLGC parameters contain all the information of series and parallel losses -already separated- and inherently they are derived by making a single assumption which is the Quasi-TEM mode field approximation.

3.0 Theory

Let's first examine the mathematics to determine if obtaining the RLGC parameters directly is theoretically feasible. The well known second-order telegrapher equation is shown in (1) and it's accompanying solution is shown in (2)

$$(1) \quad \frac{d^2 V(z)}{dz^2} = \gamma^2 V(z) \quad \frac{d^2 I(z)}{dz^2} = \gamma^2 I(z)$$

$$(2) \quad \begin{aligned} V(z) &= V^+ e^{-\gamma z} + V^- e^{\gamma z} \\ I(z) &= I^+ e^{-\gamma z} + I^- e^{\gamma z} \end{aligned} \quad I(z) = \frac{V^+}{Z_c} e^{-\gamma z} - \frac{V^-}{Z_c} e^{\gamma z}$$

The concept of complex propagation constant and characteristic impedances are introduced and based on the RLGC parameters from a physical transmission line they look as shown in (3)

$$(3) \quad \begin{aligned} \gamma &= \sqrt{z \cdot y} = \sqrt{(r + j\omega l) \cdot (g + j\omega c)} \\ &= \alpha + j\beta \end{aligned} \quad Z_c = \sqrt{\frac{z}{y}} = \sqrt{\frac{(r + j\omega l)}{(g + j\omega c)}}$$

where α is the attenuation in neper/meter, and β is the phase constant in radian/meter.

We also know that we can obtain a chain or ABCD matrix (4) from S-parameters measurements with a simple transformation. The main attribute of the chain matrix is that expresses $[V_1, I_1]$ at the output port with respect to the $[V_0, I_0]$ at the input port. In our transmission line case, the length separation between input and output port is denoted by the length "l".

$$(4) \quad \begin{bmatrix} V_1 \\ I_1 \end{bmatrix} = \begin{bmatrix} A & B \\ C & D \end{bmatrix} \cdot \begin{bmatrix} V_0 \\ I_0 \end{bmatrix}$$

By expressing (2) in matrix form, we get (5)

$$(5) \quad \begin{bmatrix} V_1 \\ I_1 \end{bmatrix} = \begin{bmatrix} e^{-\gamma \cdot l} & e^{\gamma \cdot l} \\ \frac{e^{-\gamma \cdot l}}{Z_c} & -\frac{e^{\gamma \cdot l}}{Z_c} \end{bmatrix} \cdot \begin{bmatrix} V^+ \\ I^+ \end{bmatrix}$$

Expressing $[V_0, I_0]$ in terms of $[V^+, V^-]$ can be done by evaluating (5) with a length of 0. If we then invert and express $[V^+, V^-]$ as a function of $[V_0, I_0]$ we obtain (6)

$$(6) \quad \begin{bmatrix} V^+ \\ V^- \end{bmatrix} = \begin{bmatrix} \frac{1}{2} & \frac{Z_c}{2} \\ \frac{1}{2} & -\frac{Z_c}{2} \end{bmatrix} \cdot \begin{bmatrix} V_0 \\ I_0 \end{bmatrix}$$

by multiplying (5) and (6) we obtain the final transmission line chain matrix in (7)

$$(7) \quad \begin{bmatrix} V_1 \\ I_1 \end{bmatrix} = \begin{bmatrix} \cosh(\gamma \cdot l) & -Z_c \cdot \sinh(\gamma \cdot l) \\ -\frac{\sinh(\gamma \cdot l)}{Z_c} & \cosh(\gamma \cdot l) \end{bmatrix} \cdot \begin{bmatrix} V_0 \\ I_0 \end{bmatrix}$$

$$\cosh(\gamma l) = \frac{e^{\gamma l} + e^{-\gamma l}}{2}$$

$$\sinh(\gamma l) = \frac{e^{\gamma l} - e^{-\gamma l}}{2}$$

In summary: if we are able to either measure or simulate S-parameters after the chain matrix is computed, we can then readily extract the inherent properties of the transmission line by simply computing the complex propagation constant γ and the complex characteristic impedance Z_c , as shown in (8)

$$(8) \quad \gamma = \frac{\text{arc_cosh}(A)}{l} \quad Z_c = \sqrt{\frac{B}{C}}$$

Finally, we obtain the RLGC parameters as shown in (9)

$$(9) \quad \begin{aligned} z &= r + j\omega l = Z_c \cdot \gamma & y &= g + j\omega c = \frac{\gamma}{Z_c} \\ r &= \text{Re}(z), l = \frac{\text{Im}(z)}{\omega} & g &= \text{Re}(y), c = \frac{\text{Im}(y)}{\omega} \end{aligned}$$

4.0 Measurement Impairments (The real world)

The derivations in the previous section work very well for clean simulated data when the only DUT in question is the transmission line. Unfortunately, real life measurements are subject to many kinds of errors and problems that make the above formulation not very robust. The measurement problem can be simplified by thinking that any DUT measurement contains two error matrices on each side as shown on *Figure 3*

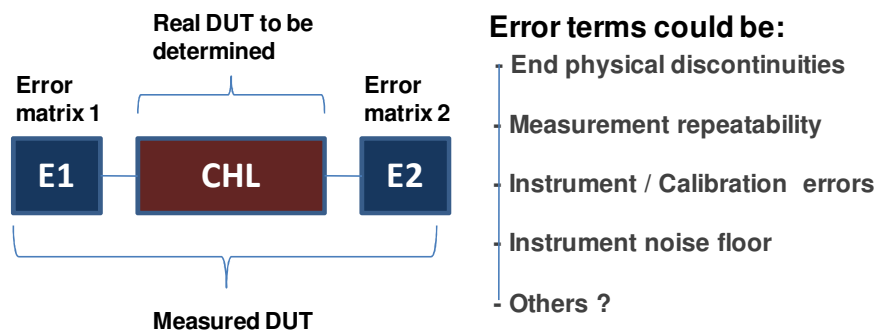


Figure 3: First order error model

The first-order error model complicates the calculation of γ and Z_c . Fortunately, by measuring two electrically equivalent transmission lines with different lengths, a trick can be played to obtain the complex propagation constant γ [9]

$$(10) \quad \begin{aligned} M1 &= E1 \cdot CH_L \cdot E2 & M1 \cdot M2^{-1} &= E1 \cdot CH_L \cdot CH_S^{-1} \cdot E1^{-1} \\ M2 &= E1 \cdot CH_S \cdot E2 & M1 \cdot M2^{-1} &= E1 \cdot CH_{(L-S)} \cdot E1^{-1} \end{aligned}$$

$$(11) \quad \begin{bmatrix} \cosh(\gamma \cdot l) & -Z_c \cdot \sinh(\gamma \cdot l) \\ -\frac{\sinh(\gamma \cdot l)}{Z_c} & \cosh(\gamma \cdot l) \end{bmatrix} = e^{\begin{bmatrix} 0 & -\gamma \cdot l \cdot Z_c \\ -\frac{\gamma \cdot l}{Z_c} & 0 \end{bmatrix}}$$

$$(12) \quad M1 \cdot M2^{-1} = E1 \cdot e^{\begin{bmatrix} 0 & -Z_c \gamma (L-S) \\ \frac{\gamma (L-S)}{Z_c} & 0 \end{bmatrix}} \cdot E1^{-1} \quad \begin{aligned} \text{Eig}(M1 \cdot M2^{-1}) &= \{e^{\gamma(L-S)}, e^{-\gamma(L-S)}\} \\ \{\pm\gamma\} &= \frac{\log(\text{Eig}(M1 \cdot M2^{-1}))}{(L-S)} \end{aligned}$$

Equations (10), (11) and (12) show that complex propagation constant per unit length can be calculated removing the error terms when an additional measurement is taken. With the correct γ , now Z_c can be calculated as shown on (13)

$$(13) \quad Z_c = \frac{-B}{\sinh(\gamma(L-S))}$$

Depending of the specific setup, this methodology makes several assumptions:

- Normally two traces on the same layer with the same characteristics are measured. This carries the assumption that these two traces have exactly the same per unit length characteristics.
- The method is also based on the assumptions that the error terms $E1$ and $E2$ are the same between the two measurements. Depending of the setup this might be true, or not. As always, we need to carefully consider and understand the assumptions before applying any methodology.
- Of course, the fundamental premise inherent in all these equations is that the transmission line is uniform and homogeneous across its length

So now, with both, the complex propagation constant and characteristic impedance determined, we can back calculate the RLGC parameters we are after.

5.0 Measurements

VNA measurements were performed in our lab to determine the trace s-parameters using the following setup:

- 40GHz VNA (E8363A)
- GSG 250um wafer probes. Ground-Signal-Ground style was selected to minimize current redistribution path around the tips of the wafer probes and hence to reduce inductive discontinuity in the launch
- SOLT calibration

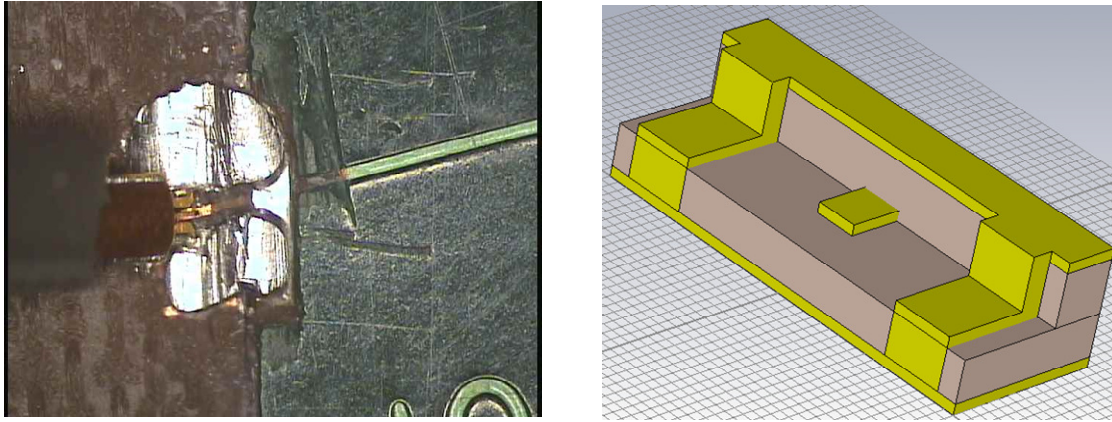


Figure 4: Wafer probe landing structure photograph (Left) and 3D model (Right).

Figure 4 (Left) shows a typical prepared sample. The board is milled down from the top until we reach the trace to measure, then the dielectric is scraped very close to the trace to build the ground walls on the sides, finally the top and bottom planes are connected as to try to minimize the plane-to-plane excitation. Only a small portion of a trace is exposed in order to land the probe (on the order of mils) - the rest of the trace should be the uniform transmission line DUT we wish to measure

Two samples were measured with different copper roughness, but the same approximate cross-section. One of the samples had a reverse treated foil, RTF, (rougher copper), while the other had a very-low-profile copper (VLP). These test boards were originally created for SPP measurements so the test boards had SMA launch structures. The samples were measured with SMA before milling the board with the intention to compare the results for the two different launch types.

Figure 5 shows the difference between these two measurements. (Please disregard the absolute value of the Insertion Loss, by milling the wafer-probe sample, we made the trace a little shorter). In terms of Insertion Loss, the SMA launch on this board is very good, we only see a little dip at around 30GHz, and then a dip at 40GHz. By looking at Insertion Loss only, one would be tempted to say that up to 20GHz these measurements are equally good. The difference in measurement quality is better observed on the return loss. Due to non-optimized connector launch, the SMA case experiences a much higher level of reflections as compared to wafer probe case. At 10GHz there is already a 10dB difference, and then the difference saturates at 20GHz with a 15dB difference approximately.

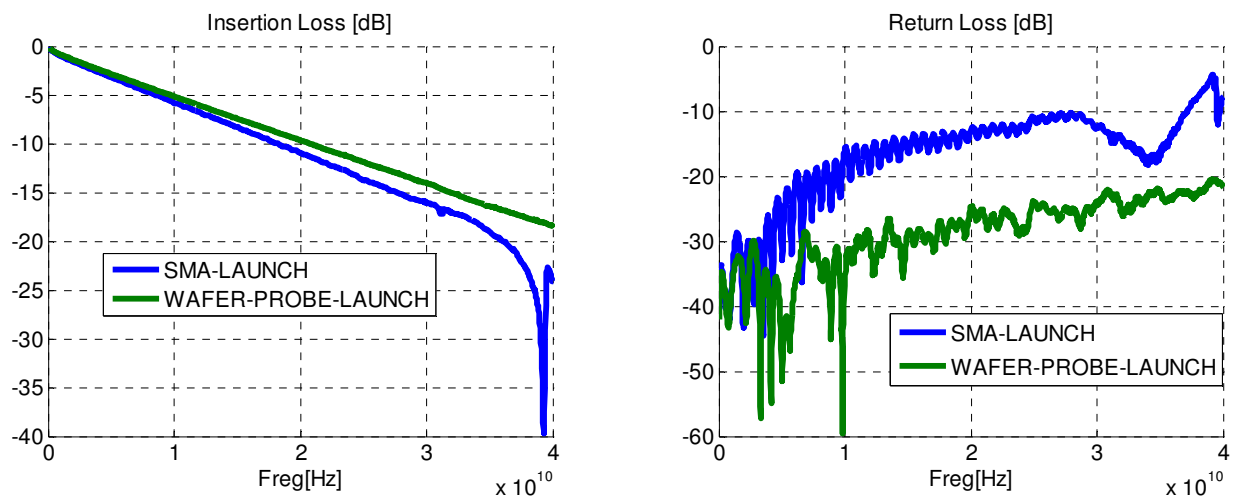


Figure 5: Insertion Loss (Left) and Return Loss (Right) measured using an SMA launch (Blue) and wafer probe launch (Green).

Going forward, throughout this paper, the analysis will continue using wafer-probe measurements only. The measurement procedure was as follows:

1. Mill the sample and prepare the ends for measurements
2. Calibrate the instrument
3. Measure the long-trace-case, forward and backward (the same sample is reversed and measured again)
4. Cut the "SAME" trace and prepare the landing for the short case
5. Measure the short case on the same trace

By measuring the same trace twice, long and short, we are attempting to remove the uncertainty of differences between different traces. In this case the only assumption we rely on is that the trace is uniform.

6.0. Characteristic Impedance by Direct Inversion

Method

As shown in Section 3.0 equation (8), just by computing the chain matrix we can extract both γ and Z_c - we'll call this the *Direct Inversion Method*. Note that for the direct Z_c calculation, γ is not required

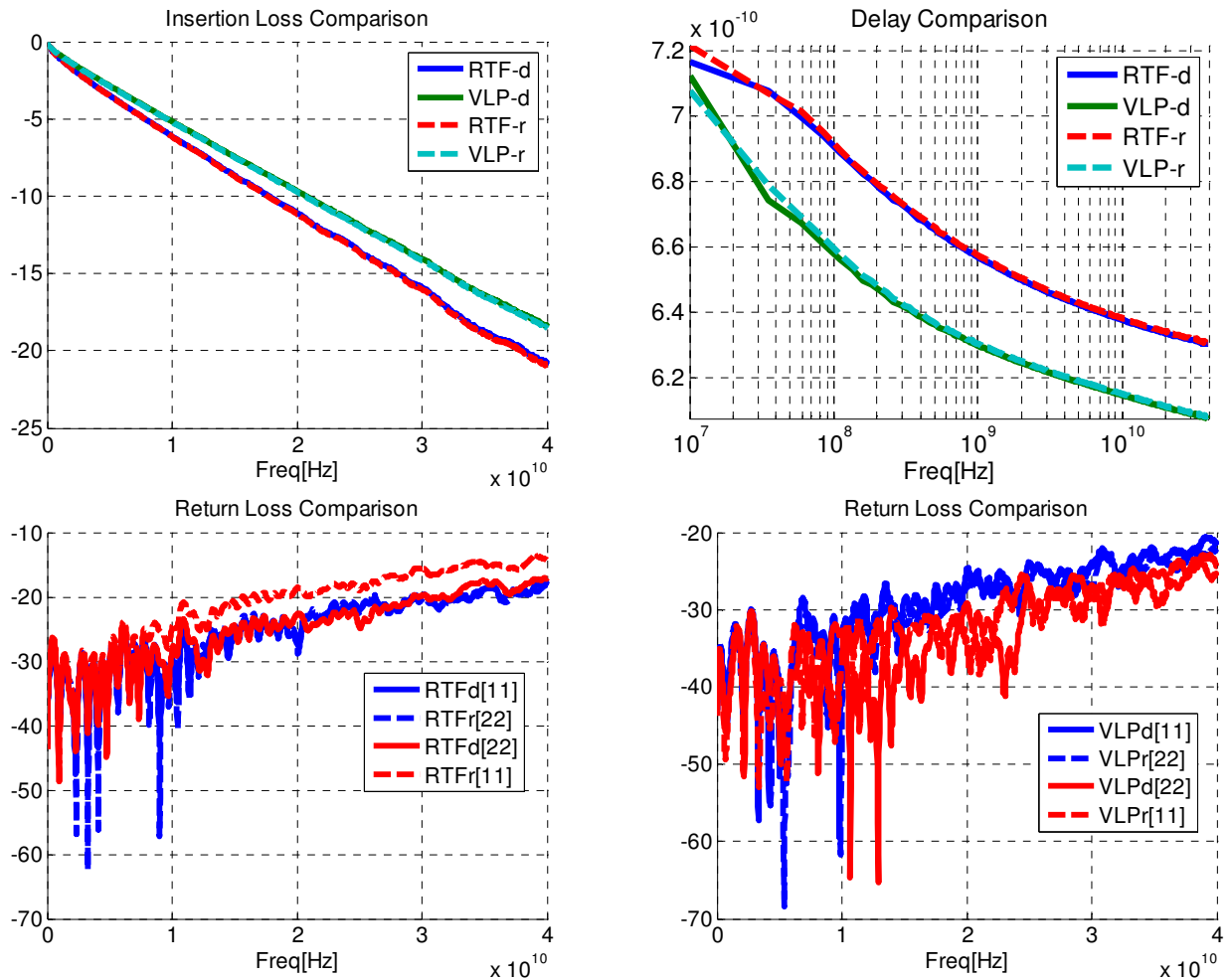


Figure 6: S-parameter comparison between VLP and RTF, both direct and reverse, (Top-left) insertion loss, (Top-right) delay, (Bottom-left) RTF return loss, (Bottom-right) VLP return loss

Before we start with the Z_c computation, let's review the S-parameter measurements for both samples. In *Figure 6*, from an S-parameter view point, the measurement looks very good.

A closer examination reveals that on the RFT sample at least one of the measurements were not as good as the others as can be seen on the RFT return loss. Note how one of the traces has a higher return loss than the others. Another observation is that the RFT sample shows higher reflection in general that VLP when looked with respect to a 50 Ohms renormalization impedance. Next, using this data, we calculate Z_c from equation (8).

In *Figure 7* the computed characteristic impedance for both RTF and VLP is shown. This waveform is rich in features, certainly not smooth and quiet as expected from a "simulated" characteristic impedance plot. Even though we have many resonances, we can still see the expected theoretical behavior. The impedance comes down, and then stays almost flat in the 1GHz to 10GHz range, slowly increasing above 20GHz.

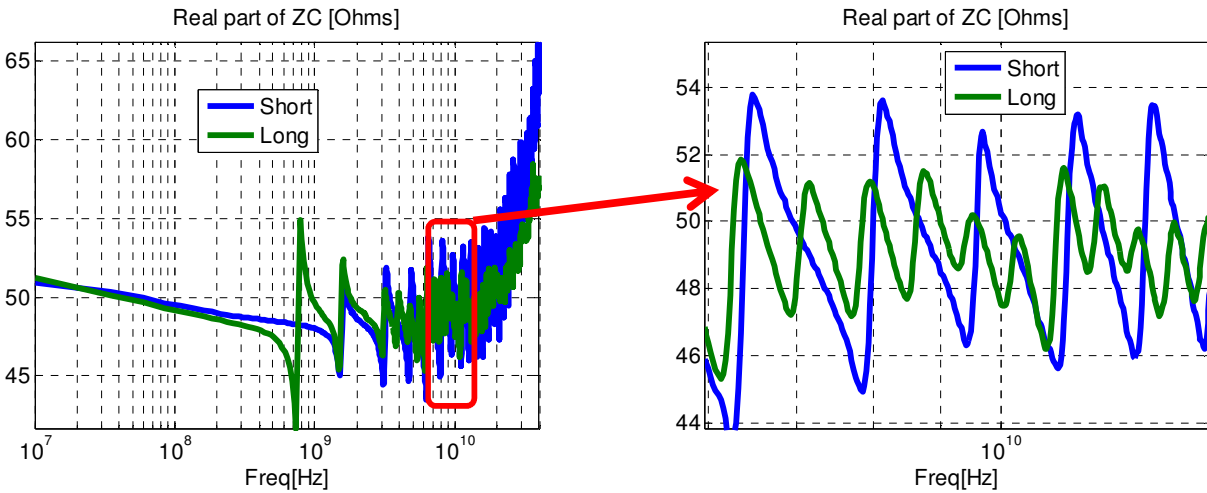


Figure 7: Real part of the characteristic impedance obtained using the direct calculation method

In *Figure 8* we observe that the imaginary part also has the expected behavior, but full of those periodical-looking resonances.

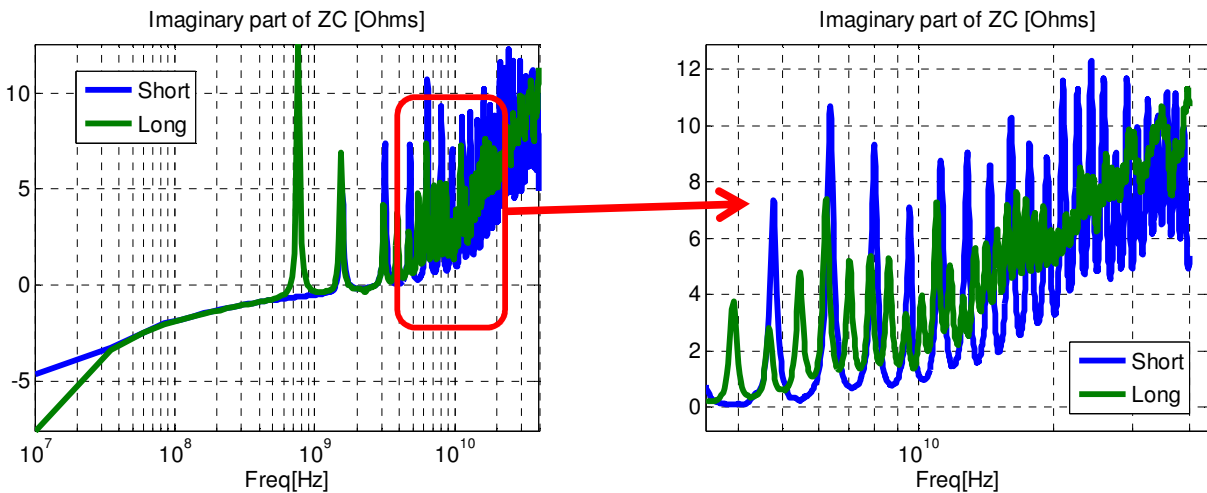


Figure 8: Imaginary part of the characteristic impedance obtained using the direct calculation method

Even though in general the characteristic impedance of the plots follows the expected trends, there are a few things that deviate from expectations:

- All the resonance peaks (where are they coming from?)
- The fact that at higher frequencies, both the real and imaginary parts are increasing a little more than expected

The remainder of this study will be dedicated to understanding these curves, and to derive different methods to extract the actual characteristic impedance in order to see if we can understand the errors and see how much we can improve upon the Direct Inversion Method.

6.0. Characteristic Impedance by Renormalization

One trick that can be played to obtain the characteristic impedance is to renormalize the S-parameters to a different (complex) impedance relying on the minimization of the return loss as an objective function.

As an illustration, *Figure 9* shows the effect of renormalization with a constant and real impedance on the S-parameters. The actual impedance of this trace is around 50 Ohms. We can see it when we change the impedance to either higher or lower values, the return loss grows and weaves start showing up on the insertion loss. This is a common and very simple way to quickly determine the equivalent characteristic impedance of a trace (or a composite structure) using the VNA data.

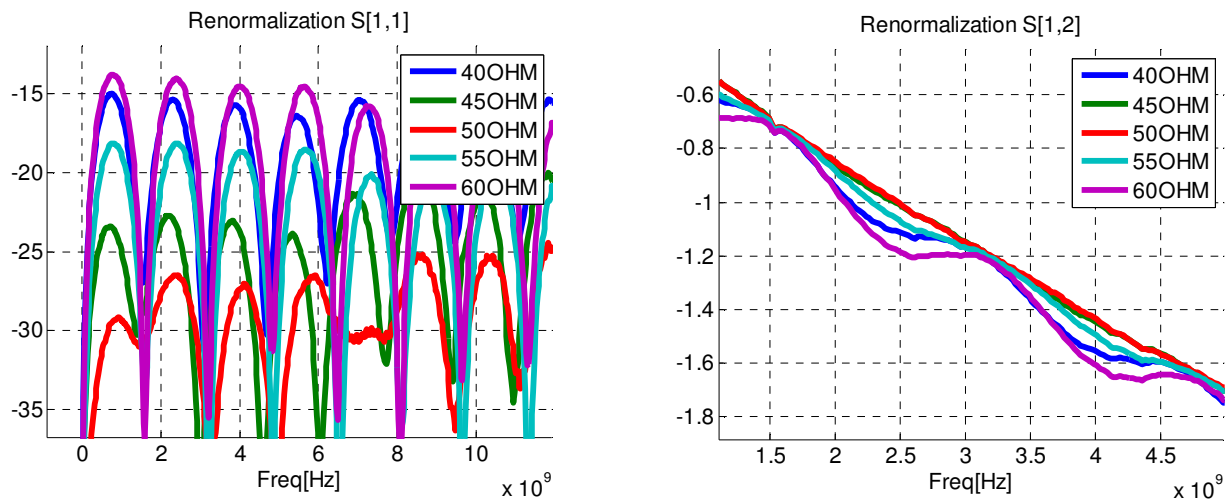


Figure 9: Effect of a simple renormalization of S-parameters, (left) Return Loss, (right), Insertion Loss

We can now expand upon this approach in two ways:

1. Allow the characteristic impedance to be a complex number
2. Also, allow the characteristic impedance to change as a function of frequency or "frequency ranges"

An automated numerical algorithm with a frequency band of 250 MHz was created to perform this calculation, meaning only one point per 250MHz will be obtained from this calculation.

Figure 10 shows the comparison of the renormalization case vs. the direct case. It can be seen that in general terms the computation of characteristic impedance using a completely different way results in very similar data - this is good news. Also the renormalized case shows less peaking and it's flatter at lower frequencies. By using frequency ranges as opposed to frequency points, we are in essence smoothing the waveform, peaks included. This is the reason for the differences both at high and low frequency between these cases.

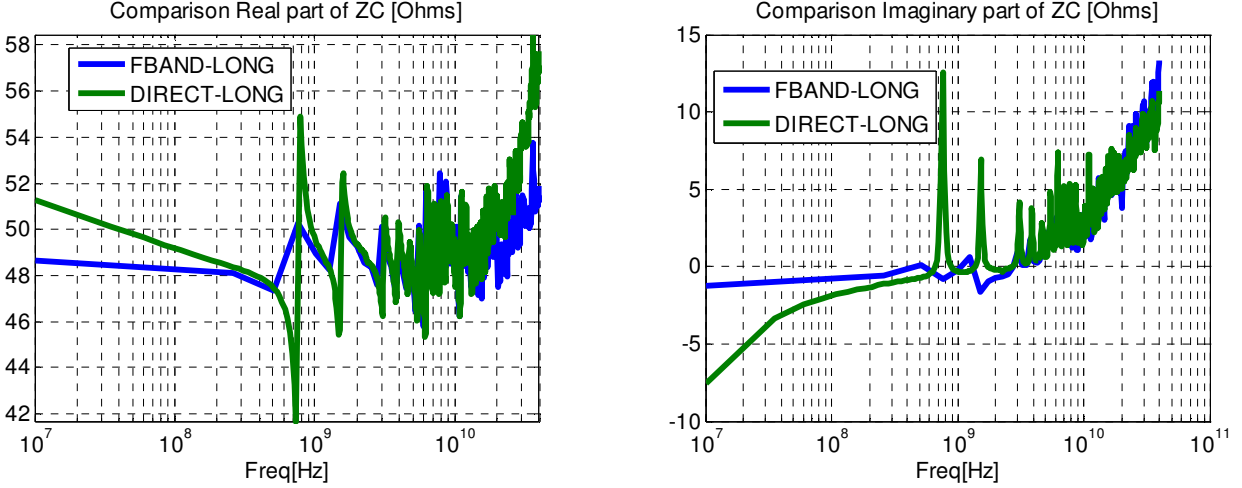


Figure 10: Characteristic impedance obtained by renormalization compared to the Direct Inversion Method, (Left) real part, (Right) imaginary part

Compared to the Direct Inversion Method, this algorithm has the advantage that for the impedance calculation only one set of data (not a short and a long) is required. The method is computationally expensive since the renormalization has to be performed at every frequency point.

From this exercise we conclude that even though we get the same result as compared to the Direct Inversion Method, which is comforting, we are not gaining much in terms of Zc quality

7.0. Characteristic Impedance by Error Model Calculation

All the observed resonances in part could be coming from the end-discontinuities. Although these resonances may be small, they are there nevertheless and we know their effect will grow with increasing frequency.

In Section 4, *Figure 3*, there are two error terms, namely (E1) and (E2), and one equation. This type of system can't be solved without an additional assumption. If we assume that the error matrices behave like RLGC elements, where the E1 (error term 1) does not need to be the same as the E2 (error term 2), an equation can be derived to remove the end discontinuities

A generic RLGC matrix will have the format shown in equation (14)

$$(14) \quad E = \begin{bmatrix} A_{e1} & B_{e1} \\ C_{e1} & D_{e1} \end{bmatrix} \cong \begin{bmatrix} 1 & z_e \\ y_e & 1 \end{bmatrix}$$

With this assumption, the characteristic impedance can be computed as shown in (15)

$$(15) \quad N = (ABCD_L) \cdot (ABCD_S)^{-1}$$

$$ye = error_matrix$$

$$Zc^2 = \frac{[(N_{11} - 1)^2 + N_{12} \cdot N_{21}] \cdot [(N_{11} + 1)^2 + N_{12} \cdot N_{21}]}{[-2 \cdot N_{21} \cdot N_{11} + ye \cdot (N_{11}^2 - N_{12} \cdot N_{21} - 1)]^2}$$

Note there is still a unknown term in the equation (ye). For most common cases $ye \ll ze$. For example referencing equation (11) for a regular 50 transmission line, the ratio between B and C will be around 2500. In our case $Ce1 = ye$, and as an initial approximation, it will be assumed to be zero.

To make sure the formulation works, a simulation case will be created, with a known Zc , then discontinuities at the end will be added, finally equation (15) will be used to derive back Zc and compare it to the original known.

Figure 11 shows the results from this exercise. On each plot there are six traces:

- $\text{real}(ZL)$ and $\text{imag}(ZL)$ are the real and imaginary part of the Zc , respectively, computed with the Direct Inversion Method (Eq 8) including the discontinuities
- $\text{real}(ZO)$, $\text{imag}(ZO)$ are the real and imaginary parts of the characteristic impedance that we want to extract, respectively. This was computed directly from simulation (no discontinuities).
- $\text{real}(Zfound)$, $\text{imag}(Zfound)$ are the extracted characteristic impedances using Equation (15) and assuming $ye=0$.

The left figure shows the case with a smaller end landing discontinuity, the right curve is similar but applying a bigger discontinuity to it. All RLGC values for the left and right discontinuities are shown in the figure caption.

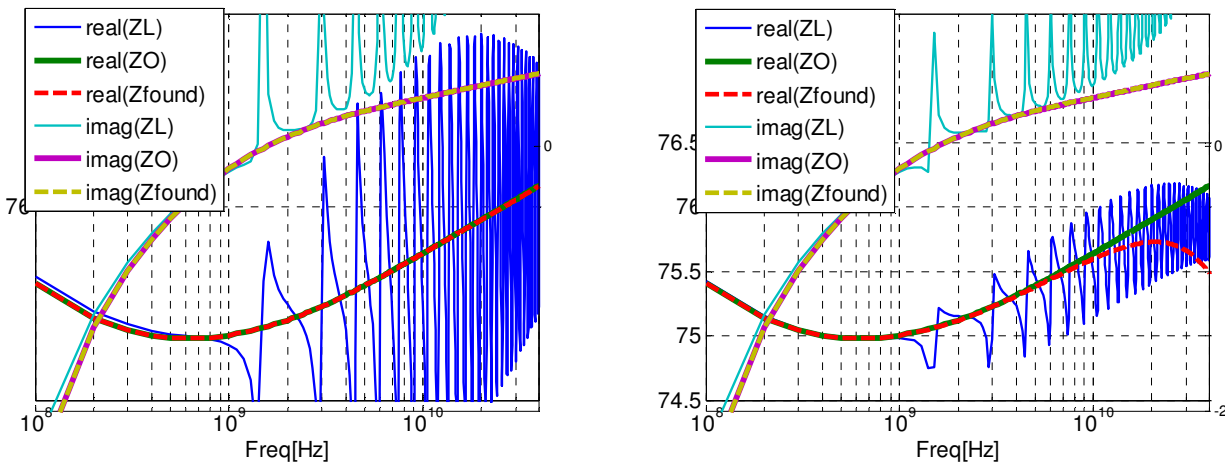


Figure 11: Simulated impedance case (Left) small landing discontinuity $RLGCa=0.001, 0.03nH, 0.5fF, 1e-5$ $RLGCb=0.002, 0.01nH, 0.5fF, 1e-5$, (Right) bigger landing discontinuity $RLGCa=0.001, 0.03nH, 50fF, 1e-3$ $RLGCb=0.002, 0.01nH, 50fF, 1e-3$

From this simple example we note that adding discontinuities to the ends, does produce an impedance profile very similar to the impedance profile we measured, telling us that maybe the characteristic impedance peaks and valleys in our measured data are simply due to the end landing discontinuities.

We also note that if the error terms were only due to the landing, for reasonable values of discontinuities, we should be able to extract the impedance perfectly without problems, even assuming $Ce1=0$.

Finally we see that, as we start increasing the end landing discontinuity, (particularly the C term) the assumption does not hold valid anymore for the entire frequency range. In this case, the C term is increased 100 times, and even though on the right figure we see the calculated Zc dropping at higher frequencies, it is still remarkably good up to 10GHz on the real part and up to 40GHz on the imaginary part.

If this method is used on measurement data, as shown on Figure 12, it can be observed that the calculated Zc is not as clean as desired. On the real part, the first resonance is higher, but then it tries to correct it and the peak to peak oscillations are reduced. The effect can be better seen on the imaginary part, where more clearly the peaks are reduced at least up to 10GHz.

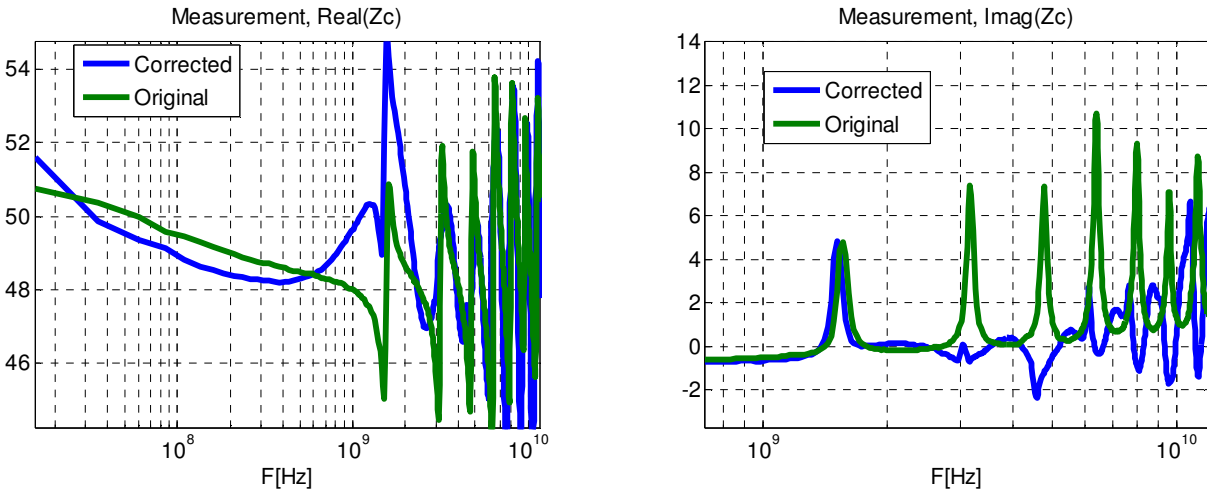


Figure 12: Z_c original vs. corrected using the error-term equation, (Right) real part, (Left) imaginary part

We hoped that this method was going to clean up the curve much better than it did. Next we move on to try to understand a bit more of the origin of the peaks and the errors in general

8.0. Characteristic Impedance by Maximum Identification

As shown in Equation (8), from the ABCD matrix, B and C are the primary elements required to calculate the characteristic impedance. In this section we'll look in more detail at the B and C elements to try to understand where the characteristic impedance resonances are coming from and what parts of the B and C parameters give us the frequency dependent nature of the characteristic impedance

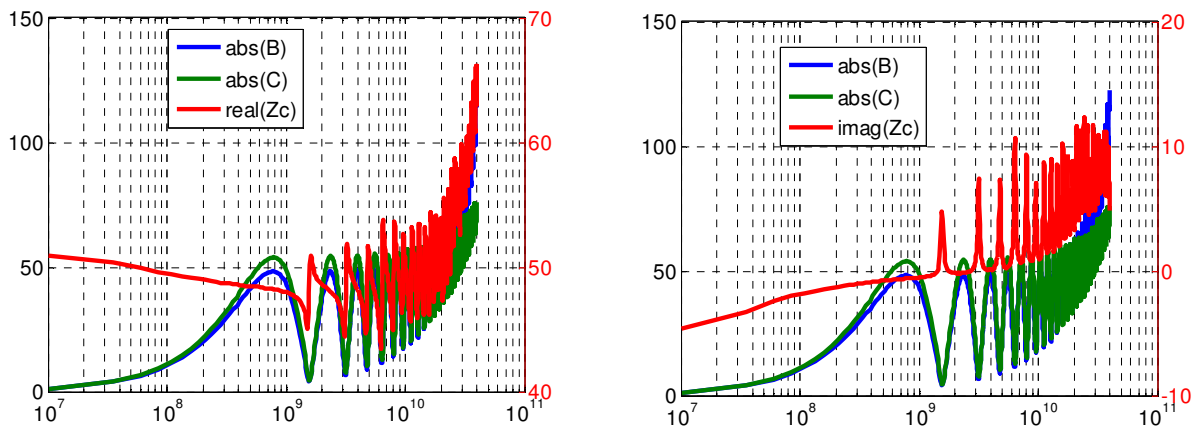


Figure 13: B & C plotted with the (Left) real part and (Right) imaginary part of the characteristic impedance

First, let's try to determine what causes the peaks on the characteristic impedance plot. In Figure 13 we can see that for both the real and imaginary parts of Z_c the peaks align exactly when both B and C dip down at multiples of the half wave resonance point. These points have a great numerical sensitivity unless the peaks are perfectly aligned and without noise, as is the case of simulated data. "C" has been scaled by 2600 in order to be compared against B on the plot. Remember that for chain matrices with reasonable values of Z_c (in the order of 50 Ohms), C is much smaller than B (three order of magnitude). This observation was used on Section 7 to calculate the error terms.

Now the calculation of γ will be performed based on equation (12). In *Figure 14* γ is shown computed for both RTF and VLP samples. The RTF measurements show oscillations in the complex propagation constant. It's possible that one of the wafer probes' GSG grounds was not properly touching GND on the sample. We'll use this data regardless, since we can still see that up to 20GHz it behaves very well and it also represents reality of the measurements. Additionally these curves can be easily fitted as shown in the figure with the dash lines.

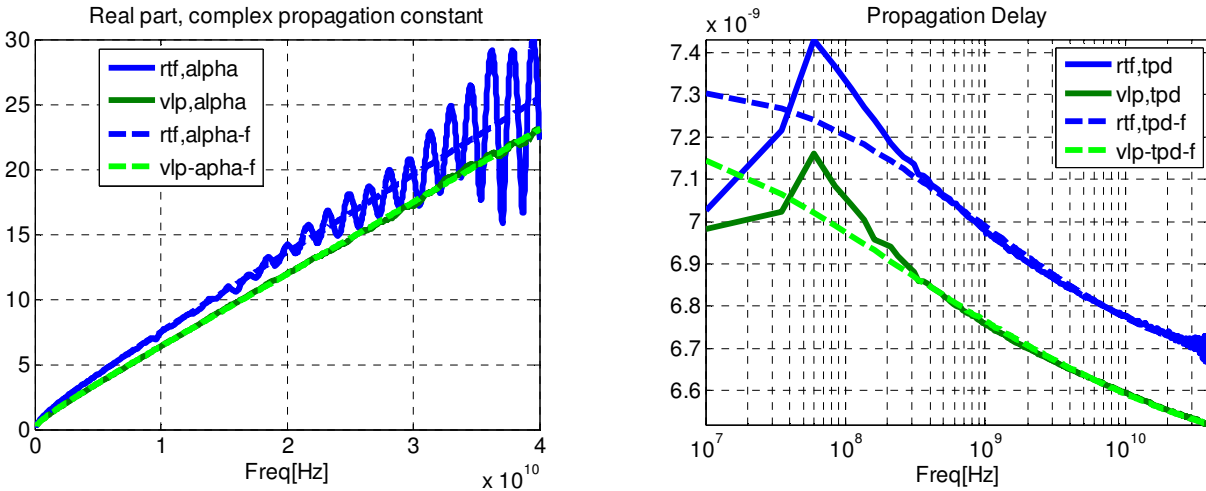


Figure 14: Complex propagation constant calculated for RTF and VLP, based on Equation (12). (Left), attenuation, (Right), propagation delay ($\beta/(2*\pi*f)$)

In *Figure 15* B & C are shown. As expected, they behaved as a sine function multiplied by a frequency dependent constant. The two upper figures show three curves. The real part of (B) is measured for the RTF sample, then an algorithm was used to identify all the maxima represented by the dots on the peaks of B, and finally another curve was created by using the maxima as multipliers of a $\sin(\gamma)$ function, where γ is the calculated complex propagation constant shown on *Figure 14*.

Since now it has been identified that the dips on B and C have high numerical sensitivity, a new method can be crafted that only selects the peaks of B and C, hence staying away from the sensitive dips. A reduced number of points will be obtained, but they should be more than sufficient to characterize and understand the frequency behavior of the characteristic impedance. The bottom two curves of *Figure 15* show a simple linear interpolation between the maximum points for the real and imaginary part of B and C. The stray point on the bottom-left is a maximum erroneously identified by the algorithm

Since we know the characteristic impedance, Z_c , can be obtained from Equation (8), it's clear that these four curves contain all the impedance information we need without really any manipulations to the data. Just by creating a B and C with only the maximum points and taking the square root of B_{max}/C_{max} , we should get the actual Z_c at those maxima. Also, by doing the same thing, but now using the "recreated" $B_{max}.\sinh(\gamma)$, we should be able to create another Z_c , now using all the points.

So in summary, from the above discussion, Z_c can be calculated in three different ways:

1. The Direct Inversion Method, i.e., simply calculating $Z_c = \sqrt{B/C}$
2. Identifying only the maxima and creating a new B_m and C_m and applying $Z_c = \sqrt{B_m / C_m}$
3. Using the maxima as a multiplier of a $\sin(\gamma)$ function, and recreate the B_r and C_r using the computed γ from Equation (12), then with the recreated B_r and C_r compute $Z_c = \sqrt{B_r / C_r}$

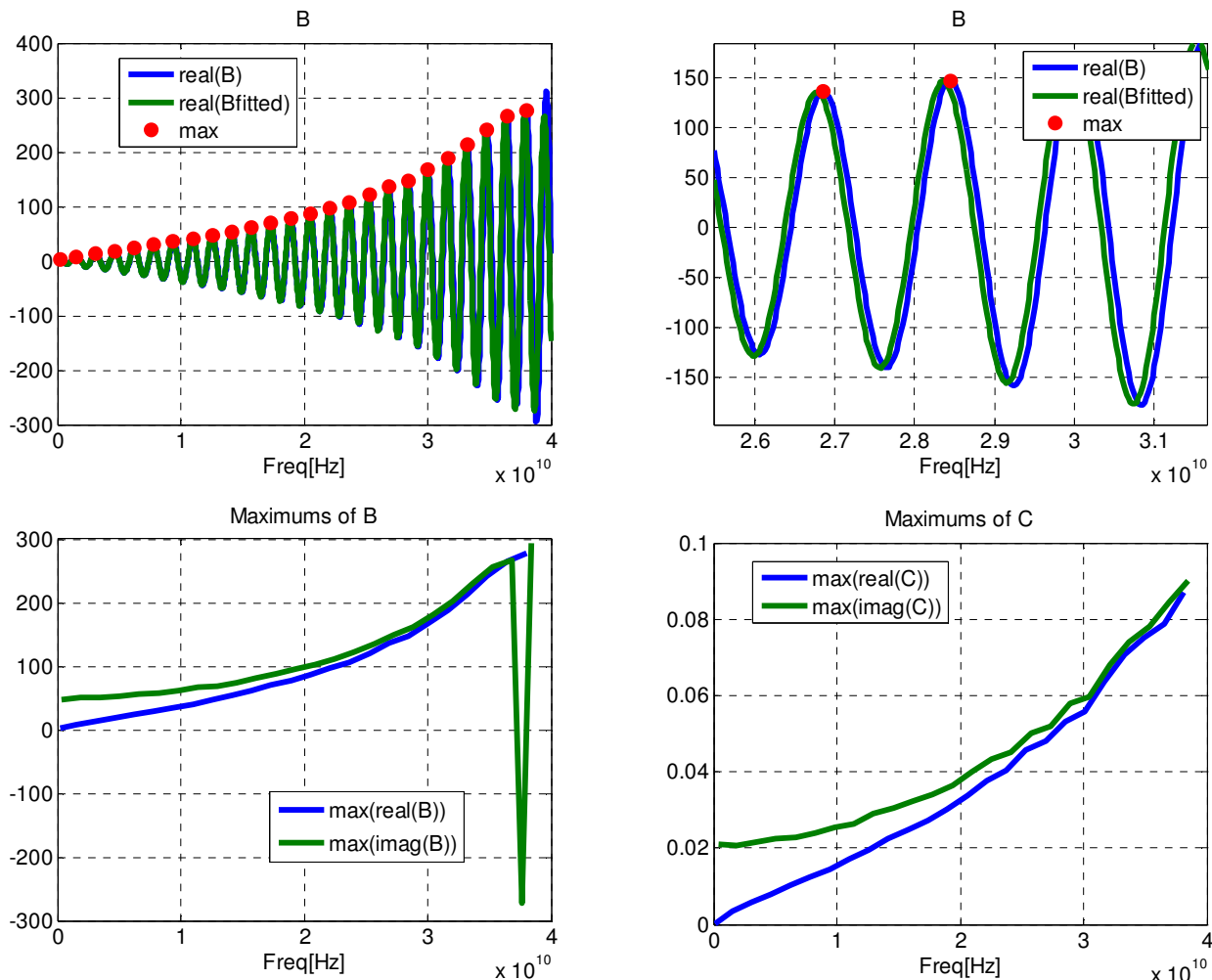


Figure 15: B & C parameters and maximum identifications. (Top-Left) B as measured, B based on calculated γ , and maximum identification on measured B , (top-right), zoomed-in version of top-left, (bottom-left), maximum only with linear interpolation for the real and imaginary part of B , (bottom-right), maximum only with linear interpolation for the real and imaginary part of C

Figure 16 shows this comparison, both for the real (Left) and imaginary (Right) part of the characteristic impedance. It is very interesting and sort of expected to see that for the maximum curve most of the oscillations have been filtered. The additional interesting observation is that for the recreated sine waveform we still see some small level of peaking but many of the oscillations have been removed. Most interesting of all is the fact that by simply selecting the maxima on B and C , the imaginary part has been corrected and looks much closer to expectations and the curve does not show the up slope at higher frequencies. However, at low frequencies the calculated Z_c still does not follow the expected behavior. This is due to the lack of data points for the maximums at low frequencies, and also due to the absolute values of B and C . At low frequencies the values of the maximums are very small, so for any absolute level of noise, the percentage error will grow.

It's important to note that at this point, computing Z_c by simply selecting the maxima, or by reconstructing the waveform by using the measured γ , produce very similar results, namely peaks are filtered and the curve trend, particularly the imaginary part is corrected. We could say that approximately from 1GHz to 20GHz this curve can be used as is, to compute RLGC parameters. But before we do that, let's look at another way of approaching the problem.

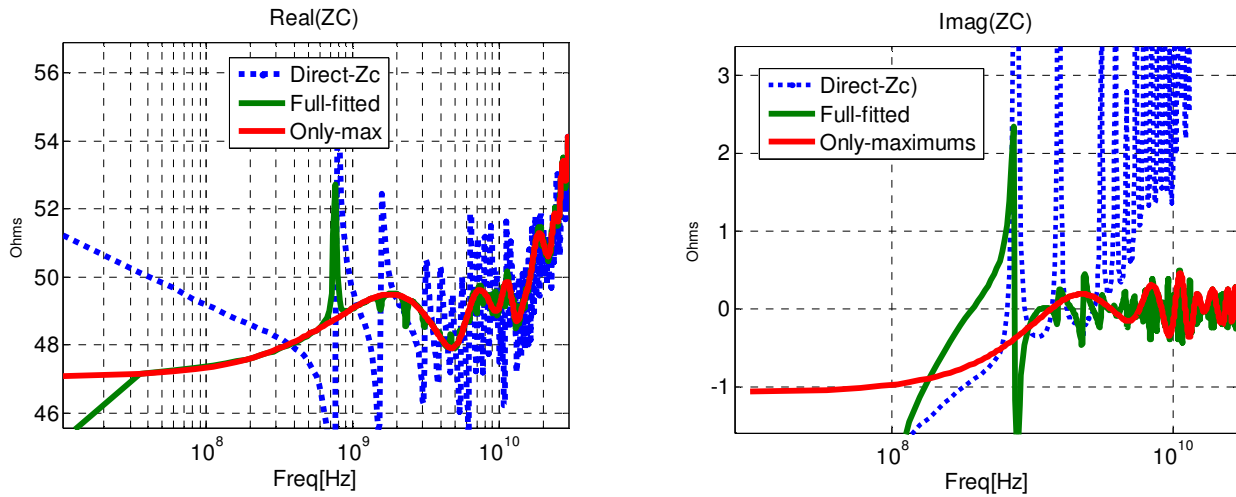


Figure 16: Direct Zc calculation method, using only maximum, and with sine function recreation, (left) real part, (Right) imaginary part.

9.0. Characteristic Impedance by Frequency Adjustment

In the previous section, it was shown that resonances seen on the characteristic impedance plot are due to the fact that dips of B and C do not exactly line up. We can introduce another algorithm that could identify those differences in the frequency domain, and then adjust the frequency domain B and C curves to make sure the dips are perfectly aligned. Figure 17 shows the inverted B and C scaled by 2600, with their maxima (actually minima since B and C have been inverted) identified. On the zoomed version we can see a slight difference in the minimum frequency. Notice the ultra-high sensitivity of these points if not perfectly aligned. The maxima are identified by interpolating only the peaks with the intent to minimize sampling error as shown on the right plot. The maximum from the interpolation is taken as the actual maximum of the measured data.

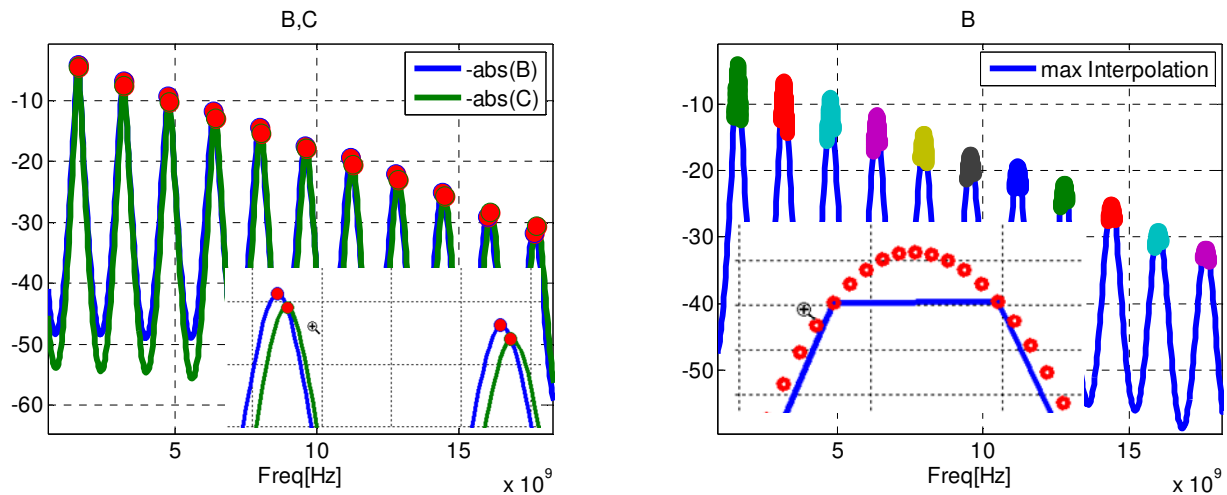


Figure 17: Frequency difference identification between B and C, (Left) B and C with maximum and zoomed version where the difference in frequency could be observed, (Right), maximum identification and interpolation only on the max to obtain the real maximum minimizing sampling error

In *Figure 18* the frequency difference between the B and C dips are plotted for the short measured transmission line (the long line behaves in a similar fashion). It's very interesting and peculiar to see that on both lines the RTF sample exhibits a steeper frequency difference between B and C than the VLP sample.

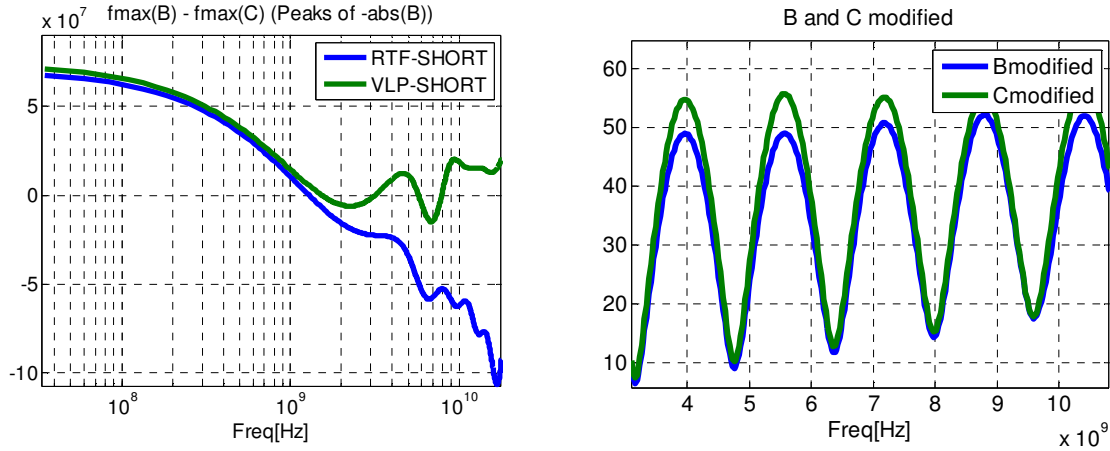


Figure 18: Shows the difference in frequency at the minimum between B and C chain matrix parameters over the frequency range. (Left) RTF vs. VLP short line, (Right), B and C adjusted to the same minimum

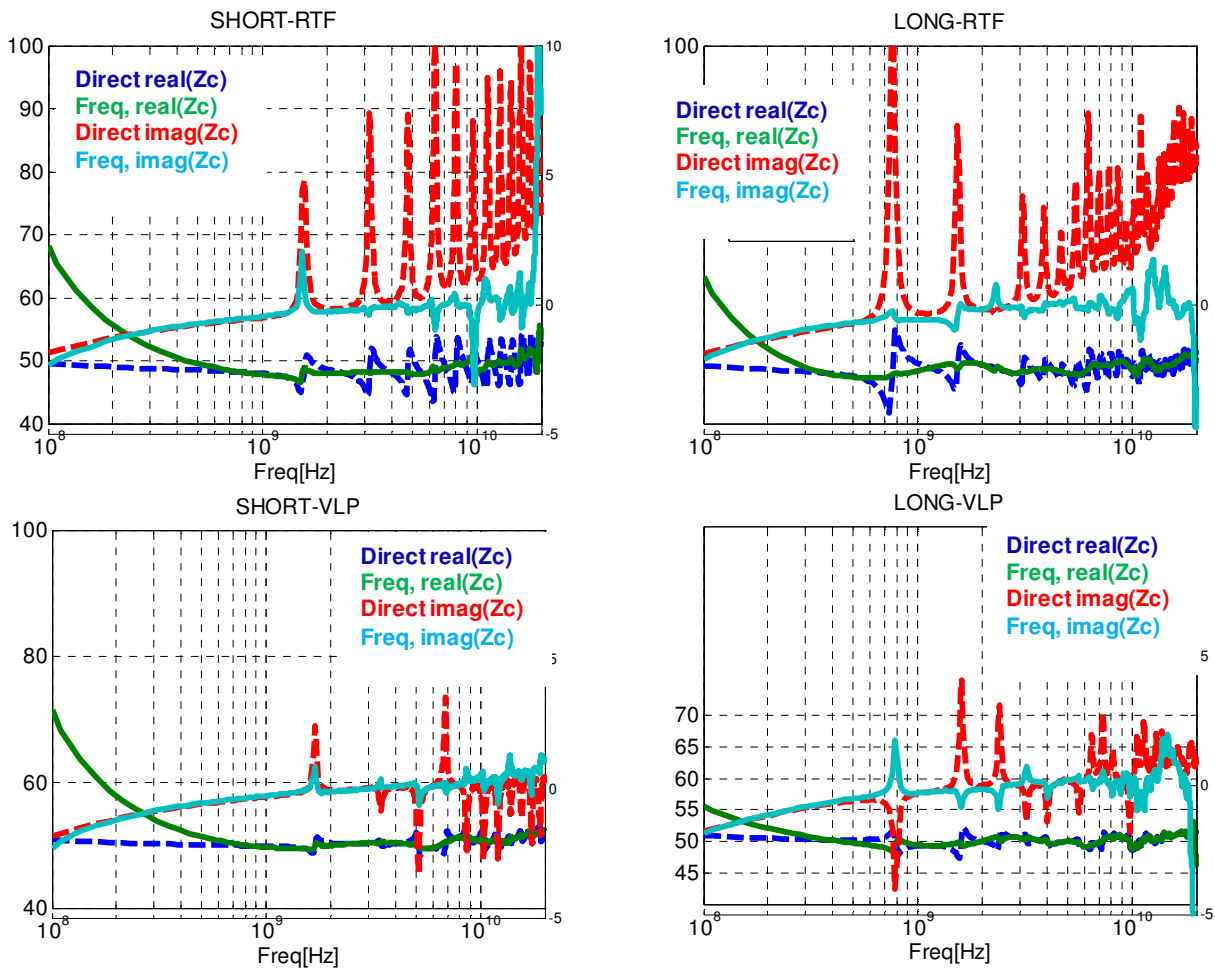


Figure 19: Direct Characteristic Impedance (real and imaginary), vs. frequency adjusted method, (Top-left) short RTF sample, (Top-right), long RTF sample, (Bottom-left) short VLP, (Bottom-right) long VLP

Note that the RTF sample in theory is rougher and with more series resistance over frequency than the VLP sample. Since we know that frequency on the B and C parameters is directly related to delay, one can speculate that there is a higher delay error on the rougher sample. Overall for every sample, we see an approximately constant relative frequency error of the order of 0.2%. On the right plot, the fixed frequency adjusted B and C are shown. Note that by forcing the dips to align in frequency, the rest of the curve gets slightly deformed.

At this point we have another Bf and Cf (the subscript “f” is used to indicate frequency adjustment). With these new parameters, Zc can be recalculated and it's shown in *Figure 19*. This step made a big difference on the impedance profile. Now we can see that almost all the peaks have virtually disappeared from the impedance plot. The same behavior can be reproduced on all the samples. With this case we are still using *all* frequency points from the waveform and not pick and choose. The only modification made was to readjust the frequency to match the dips between B and C, no other manipulations have been performed on these measurements.

11.0. RLGC Calculation

So far several different techniques have been used to retrieve the Characteristic Impedance. From the methods looked at, two of them resulted in a smoother line; both of those methods will be used to compute the RLGC parameters, and from there we will calculate the loss tangent:

- Characteristic impedance by maximum identification
- Characteristic impedance by frequency adjustment

Figure 20 shows the extracted RLGC for the RTF sample up to 40GHz.

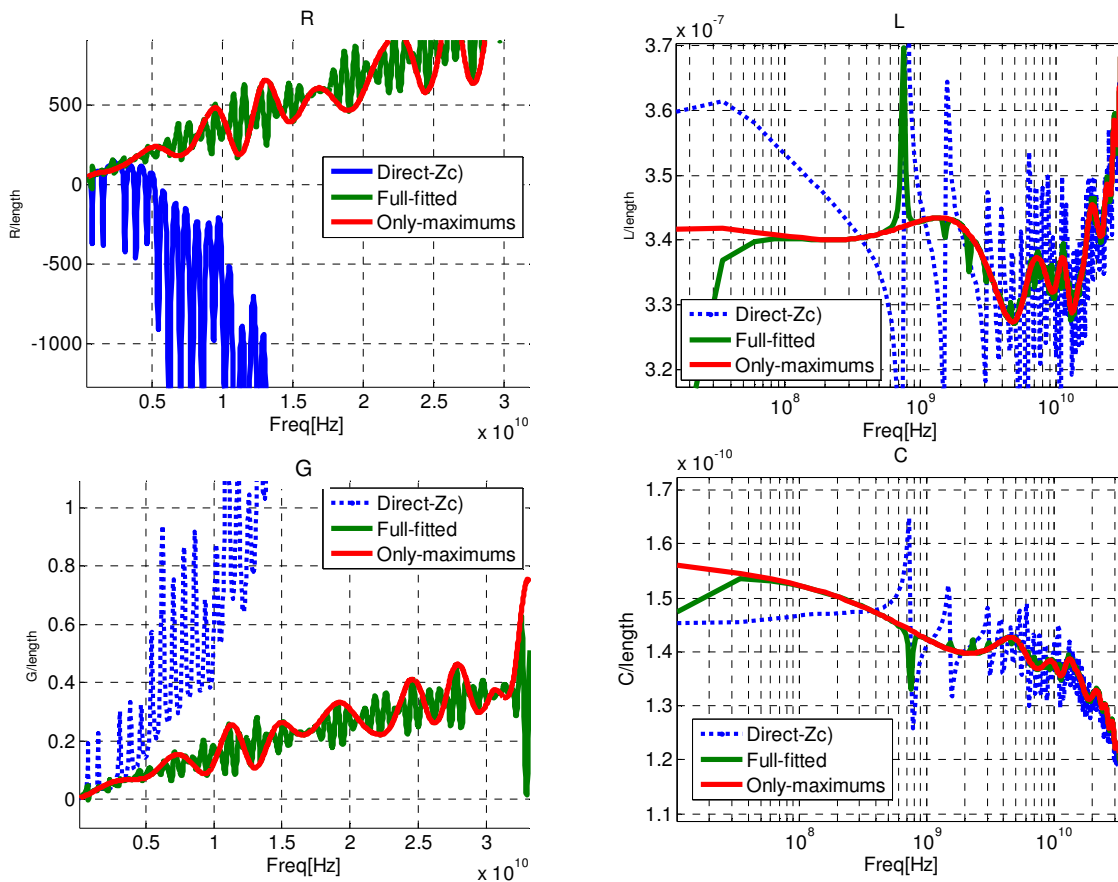


Figure 20: (Top-left) R, (Top-right) L, (Bottom-left) G, (Bottom-right) C parameters extracted from the direct method and compared to characteristic impedance by maximums and by recreating the curve with $\sin(\gamma)$

We can see a dramatic correction particularly on R and G. As can be seen, R, G, L and C behave close to expectation. These curves have been obtained without any fitting other than identifying the maxima of B and C.

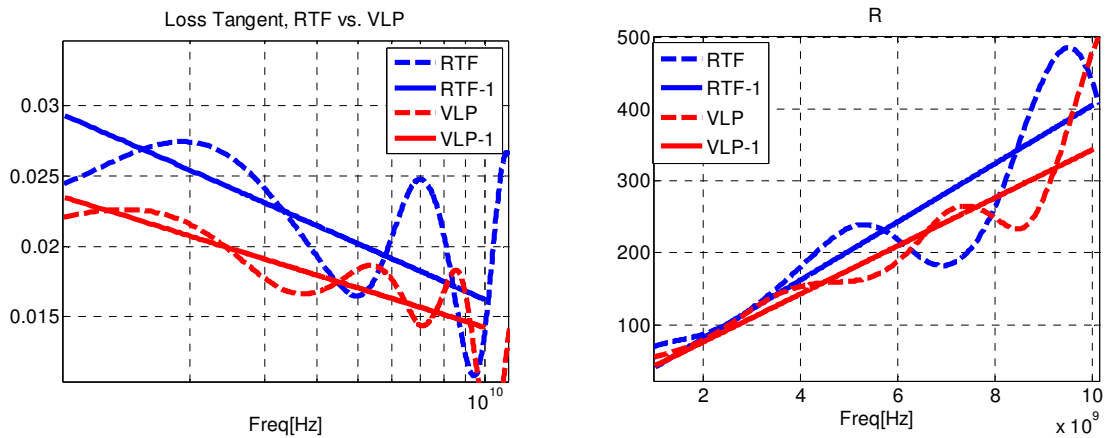


Figure 21: Comparison between RTF and VLP using maximum identification method, (Left) loss tangent, (Right) series resistance

If we compare the RTF to the VLP samples as shown on Figure 21, we can see that the loss tangent shows a downward slope around 0.023. We also note that the series resistance, including surface roughness, shows the RTF sample with a higher series resistance than VLP, as expected. On top of these curves a linear curve has been interpolated just to observe the trends.

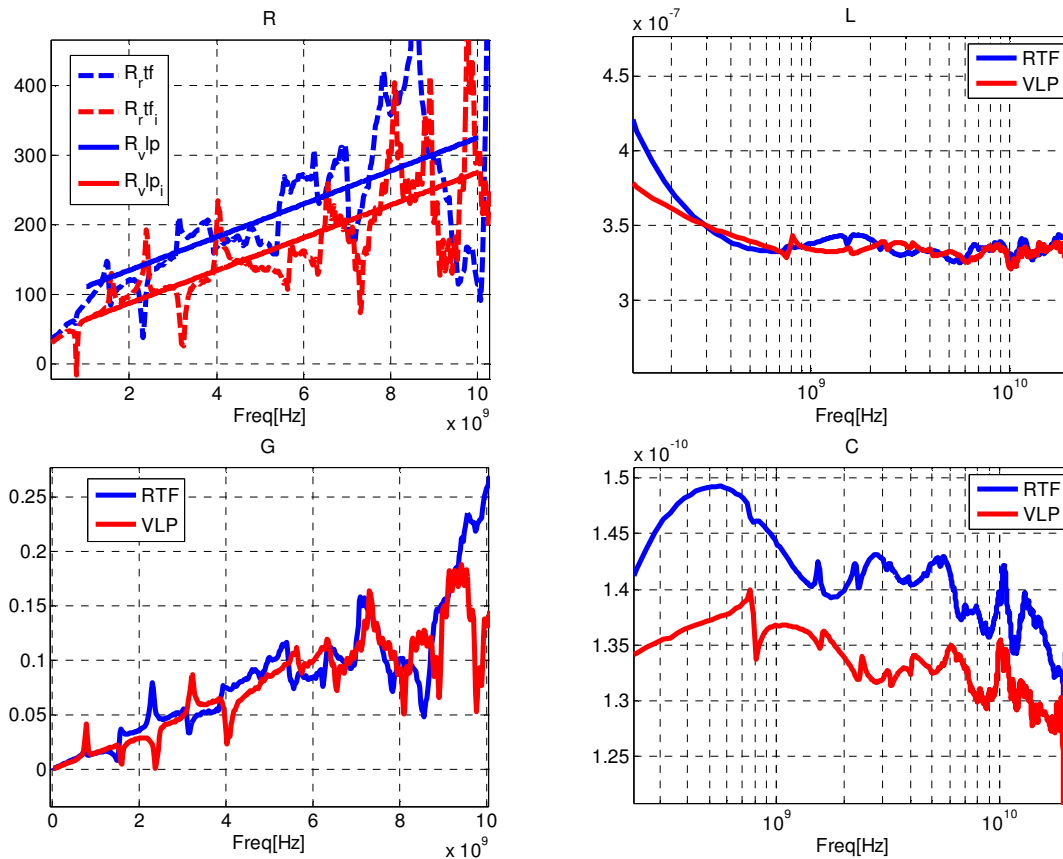


Figure 22 : (Top-left) R, (Top-right) L, (Bottom-left) G, (Bottom-right) C parameters extracted from the frequency adjustment method

The RLGC parameters using the Frequency Adjustment Methodology are shown in *Figure 22*. The same 1GHz to 10GHz interpolation was done. We again see similar trends, where the RTF sample has higher series resistance than VLP and G seems very straight and exactly the same between the two samples up to approximately 8GHz.

In

Figure 23 the loss tangent results are also shown. It can be seen that the curve looks very flat in a wide frequency range. The simple linear interpolation results on a flat or slightly tilted upward curve between 1GHz to 10GHz. The absolute value of loss tangent is around 0.02.

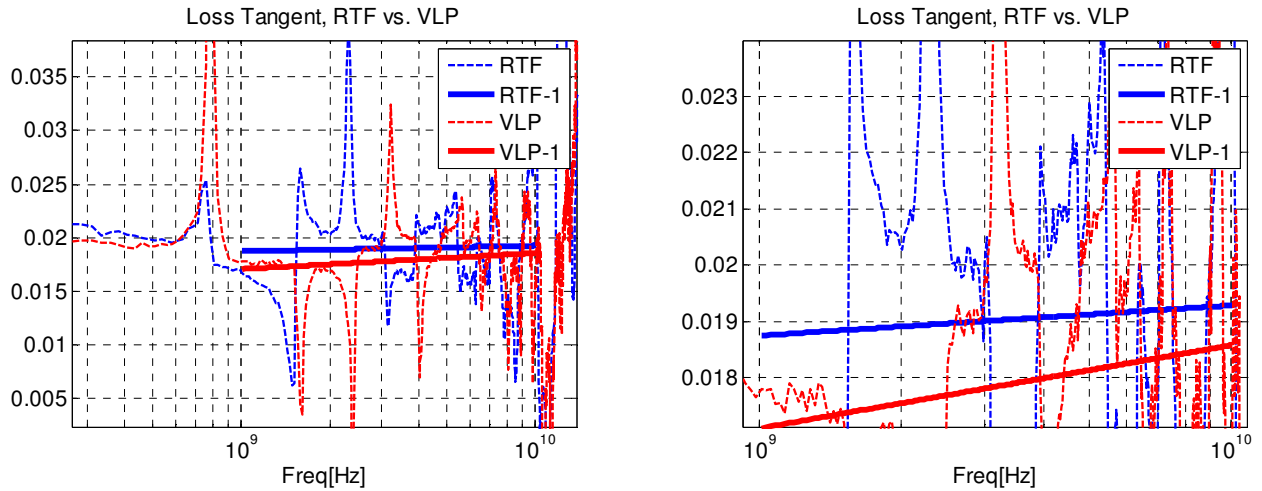


Figure 23: Loss tangent comparison between RTF and VLP using the frequency adjustment method

11.0. Summary and Conclusion

When we started working on this paper, our goal was to understand enough to be able to create a good comprehensive model of a transmission line including surface roughness. As we started to dig deeper we quickly realized that the challenge was not necessary creating the model, since there are already several models that are good approximations to the problem, but rather being able to identify and separate from measurements copper losses, versus dielectric losses. All the methodologies used up to this point heavily rely on simulation models, but none attempts to really measure and separate the losses.

With this work we attempted to walk the first steps towards this understanding

Acknowledgement

The authors wish to extend their thanks to Eugene Whitcomb (ORACLE) for his help in creating and preparing the sample structures.

References

- [1] Permittivity and Loss Tangent, Parallel Plate, 1 MHz to 1.5 GHz IPC TM-650-2.5.5.9
- [2] Stripline Test for Permittivity and Loss Tangent (Dielectric Constant and Dissipation Factor) at X-Band, IPC TM-650-2.5.5.5 and Stripline Test for Complex Relative Permittivity of Circuit Board Materials to 14 GHz, IPC TM-650-2.5.5.5.1
- [3] Test Methods to Determine the Amount of Signal Loss on Printed Boards (PBs), IPC TM-650-2.5.5.12
- [4] Jeff Loyer, "SET2DIL: Method to Derive Differential Insertion Loss from Single-Ended TDR/TDT Measurements," DesignCon2010, Santa Clara, CA, February 1-4, 2010
- [5] Deutsch, et al., "Application of the Short-Pulse Propagation Technique for Broadband Characterization of PCB and Other Interconnect Technologies," IEEE Tr. On EMC, Vol. 52, No.2, May 2010, pp. 266-287.
- [6] Hinckley, et al., "Introduction and Comparison of an Alternate Methodology for Measuring Loss Tangent of PCB Laminates," DesignCon2010, Santa Clara, CA, February 1-4, 2010
- [7] A. Djordjevic, et.al., "Wideband Frequency-Domain Characterization of FR-4 and Time-Domain Causality," IEEE. Tr. EMC, Nov. 2001, p.662
- [8] E. Hammerstad and O. Jensen, "Accurate models of computer aided microstrip design," IEEE MTT-S Symposium Digest, p. 407, May 1980
- [9] Shlepnev, et al., "Practical Identification of Dispersive Dielectric Models with Generalized Modal S-parameters for Analysis of Interconnects in 6-100Gb/s Applications," DesignCon2010, Santa Clara, CA, February 1-4, 2010